Cancer Nanotechnology

RESEARCH Open Access

Ginsenoside compound K-loaded gold nanoparticles synthesized from *Curtobacterium proimmune* K3 exerts anti-gastric cancer effect via promoting PI3K/Akt-mediated apoptosis

Aditi Mitra Puja[1], Xingyue Xu[1,2], Rongbo Wang[1], Hoon Kim[3*] and Yeon-Ju Kim[1,3*]

*Correspondence:
saphead1106@hanmail.net;
yeonjukim@khu.ac.kr

[1] Graduate School of Biotechnology, College of Life Science, Kyung Hee University, Yongin, Gyeonggi 17104, Republic of Korea
[2] Beijing Key Laboratory of Traditional Chinese Medicine Basic Research On Prevention and Treatment for Major Diseases, Experimental Research Center, China Academy of Chinese Medical Sciences, Beijing 100700, China
[3] Department of Oriental Medicine Biotechnology, Kyung Hee University, Yongin, Gyeonggi 17104, Republic of Korea

Abstract

Background: Compound K (CK) is the minor ginsenoside present in fermented *Panax ginseng* extract. Despite the pharmacological efficacy of CK, its industrial use has been restricted due to its low water solubility and poor permeability. To overcome this defect, our study was to synthesize gold nanoparticles from CK (CK-AuNPs) to investigate their potential as anticancer candidates.

Methods: To biologically synthesize CK-AuNPs, a novel strain, *Curtobacterium proimmune* K3, was isolated from fermented ginseng beverage, then combined with CK and gold salts to biosynthesize gold nanoparticles (CurtoCK-AuNPs). Their physicochemical characteristics were evaluated using UV–Vis spectrometry, FE-TEM, EDX, elemental mapping, XRD, SAED, DLS and TGA.

Results: CurtoCK-AuNPs exerted significant selective cytotoxic effects on AGS human gastric cancer cells. Fluorescence staining with Hoechst, propidium iodide, and MitoTracker demonstrated that CurtoCK-AuNPs induce apoptosis and mitochondrial damage, respectively. Quantitative real-time PCR and western blotting analyses showed that cytotoxic effect of CurtoCK-AuNPs were involved in apoptosis, based on their activation of Bax/Bcl-2, cytochrome c, caspase 9, and caspase 3, as well as their suppression of PI3K–Akt signaling.

Conclusion: Our findings provide data for understanding the molecular mechanisms of nanoparticles; thus, providing insight into the development of alternative medications based on gold nanoparticles of ginseng-derived CK.

Keywords: Nanotechnology, Green-synthesized nanoparticle, Ginsenoside-loaded nanoparticle, Anti-cancer candidate, Mechanism of action

Background

In 2018, "Global Cancer Statistics" reported that the most common malignancy was lung (1.2 million), breast (1.05 million), colorectal (945,000), stomach (876,000), and liver (564,000) (Bray et al. 2018). Gastric cancer (GC), which is a wide-spread gastrointestinal malignancy with poor survival rates (Dang et al. 2020; Smalley et al. 2012).

Several strategies have been introduced to treat this cancer, including surgical excision, chemotherapy, and radiotherapy, but no significant improvements have been observed in the outcomes of new cases (Smalley et al. 2012). Thus, novel strategies are required to overcome malignant tumors, including GC. Owing to the unique and enhanced properties of nanoparticles, their industrial applications have been expanding widely in various therapeutic fields, including biomedical, pharmaceutical, drug delivery, and target-therapy (Heiligtag and Niederberger 2013; Shakeel et al. 2016). High selectivity, efficiency, long-term stability, and harmless against normal cells are the main advantage of using nanoparticle (Lamprecht et al. 2001; Salapa et al. 2020; Su et al. 2018). Several studies have reported that nanoparticles prepared from various materials have enhanced anticancer potential compared with the therapeutic entities they contain (Davis et al. 2008). The preparation of metallic nanoparticles using physical, chemical, and biological synthetic processes have been done via several types of metallic ions (Sekhon 2014). Particularly, in biomedical applications, diagnosis of diseases (Bhattacharya and Mukherjee 2008; Puvanakrishnan et al. 2012; Sperling et al. 2008), and medicinal purpose (Cai et al. 2008; Sýkora et al. 2010; Torres-Chavolla et al. 2010), gold nanoparticles (AuNPs) are mostly used (Rónavári et al. 2021), because of synthesis and functional compatibility, less toxic effects, and easier detection (Tiwari et al. 2011).

In recent decades, medicinal plant extracts and their active ingredients have been attracting attention as alternative medications to treat cancer, and various types of AuNPs can be biologically synthesized using plant extracts, enzymes, and microorganisms (Herizchi et al. 2016; Shakeel et al. 2016). Over the last few decades, metallic nanoparticles have garnered considerable attention and interest in the fields of research and industry. Several methods have been established to formulate nanoparticles with unique physical, chemical, and biological characteristics (Shah et al. 2015). Recently, biological synthesis has become important alternative to traditional chemical and physical methods for preparing nanoparticles (Gowramma et al. 2015). Recent articles have focused on the biological synthesis of nanoparticles using microorganisms and plants because of their safe, cost-effective, and eco-friendly features (Shunmugam et al. 2021; Zhang et al. 2018).

Ginseng which refers to the roots and rhizomes of *Panax ginseng* C. A. Meyer, is one of the oldest traditional remedy used primarily in Eastern Asia thousands of years. As major bioactive ingredients, various ginsenosides, glycosides and saponins, are known to exist in the ginseng mainly. Among the diverse ginsenosides, compound K (CK) is a minor secondary ginsenoside transformed from major ginsenosides (Sharma and Lee 2020) and can be easily absorbed compared with its major ginsenosides (Rb1, Rb2, and Rc) (Akao et al. 1998). Much health beneficial effects of CK have been demonstrated to provide anticancer, anti-inflammation, anti-atherosclerosis, anti-diabetes, anti-aging/skin protection, hepatoprotection, and neuroprotection effects. In particular, the activity of CK against malignant tumor has been widely investigated in different cancer cell types (Sharma and Lee 2020). However, the anticancer effect of microbial nanoparticle loaded with CK against gastric cancer has not been demonstrated. In addition, industrial application becomes limited of CK for poor solubility in water, poor permeability, and serious P-glycoprotein efflux (Yang et al. 2012; Zhang et al. 2012).

Apart from other synthesis methods, biological components, such as the microbiome are safe, tidy, and less time consuming (Grasso et al. 2019). Microorganism are considered a perfect alternate way to traditional green synthesis methods because of efficient production of nanoparticles. Biosynthesis of nanoparticles occurs when the microorganism captures selected ions from the environment and uses enzymes to transform metal ions into products and initiate cell activities. Based on the recent studies that not only bacteria cell themselves, but also their modified substances have shown the anticancer effects (Cao et al. 2019; Cao and Liu 2020; Liu et al. 2022; Wang et al. 2022), we hypothesized that microbial synthesis of CK-AuNPs can be effective in treating various diseases including cancers. In these situation, we previously isolated novel bacterial strain which was identified as a *Curtobacterium proimmune* K3 (NCBI accession number: MW563938) (Dhandapani et al. 2021), a Gram-positive, obligately anaerobic, rod-shaped bacterium belonging Microbacteriaceae family (Chase et al. 2016; Funke et al. 2005). Thus, the objective of this study was to formulate AuNPs from CK and to investigate their potential as anticancer candidates. To achieve this, the biological synthesis of CK-AuNPs using *C. proimmune* K3 was optimized and the mechanism underlying apoptosis signaling in GC cells was explored.

Materials and methods

Materials

Ginsenoside compound K (CK; C36H62O8, MW 622.85, CAS No. 39262-14-1) was obtained from the Ginseng bank of Kyung Hee University (Suwon, Republic of Korea). Luria–Bertani (LB) broth and agar were purchased from Oxoid (Hampshire, England). Analytical grade hydrogen tetrachloroaurate (III) hydrate ($HAuCl_4 \cdot 3H_2O$) was purchased from Sigma-Aldrich (St. Louis, MO, USA). Phosphate-buffered saline (PBS) was purchased from Biosesang (Seongnam, Republic of Korea). Roswell Park Memorial Institute-1640 medium (RPMI), Dulbecco's modified Eagle medium (DMEM), penicillin–streptomycin (PS), and fetal bovine serum (FBS) were purchased from GenDEPOT (San Antonio, TX, USA). Dimethyl sulfoxide (DMSO), crystal violet, soluble 3-(4,5-dimethylthiazol-2-yl)-2,5-diphenyltetrazolium bromide (MTT), and Hoechst 33258 were purchased from Sigma-Aldrich. Propidium iodide solution (PI) and MitoTracker Green FM were obtained from Invitrogen (Thermo Fisher Scientific, Waltham, MA, USA). The primary antibodies against PI3K, p-PI3K, Akt, p-Akt, Bax, Bcl-2, cytochrome C, caspase 9, cleaved-caspase-9, caspase 3, cleaved-caspase-9, and β-actin were obtained from Abcam (Cambridge, UK). Secondary antibodies against anti-mouse/rabbit IgG (horseradish peroxidase; HRP) were purchased from Cell Signaling Technology (Danvers, MA, USA).

Microbial source and biological synthesis of CurtoCK-AuNPs

Novel bacterial strain *C. proimmune* K3 was isolated from traditionally fermented ginseng beverage according to the previous method (Dhandapani et al. 2021). The stock of *C. proimmune* K3 was activated at 37 °C for 24 h on a solid nutritional medium containing 25 g/L LB broth and 15 g/L agar, and the bacterial pellet was inoculated to LB broth (100 mL) for mass production. The biological synthesis of AuNPs using *C. proimmune* K3 and ginsenoside CK was performed according to a previously described method with slight modifications (Dhandapani et al. 2021). In addition, various conditions were

examined with respect to concentration of CK and $HAuCl_4$, and reaction pH and time. Briefly, the pellet of *C. proimmune* K3 was washed two times with 1 mM PBS (pH 7.2) and resuspended in 10 mL of PBS. Afterward, fluctuating concentrations of CK (0.15–0.3 mM) and $HAuCl_4{\cdot}3H_2O$ (0.5–4 mM) were individually added to the suspension of *C. proimmune* K3. The CK-gold nanoparticles (CurtoCK-AuNPs) were biosynthesized under different conditions pH (3.0–8.0) and time (1–5 days) at 37 °C in the shaking incubator (Vision Scientific Co., Daejeon, Republic of Korea). Subsequently, the dark and purple-colored mixtures were sonicated for 40 min and then centrifuged at 4000 rpm for 15 min to remove the supernatant and floating materials. The nanoparticles formed by the bacterial cells were collected by centrifugation at 13,000 rpm for 20 min. The reaction conditions-dependent optimal conditions were monitored by the peak observed by UV–Vis spectrophotometry (Spectronic Genesys 6, Cortson, UK) in the range of 300–800 nm. Collected pellets were washed twice with distilled water, and the resulting CurtoCK-AuNPs were air-dried overnight to obtain the solid specimens.

Physiochemical analyses for characterization of nanoparticles

The shape, molecular size, and distribution of nanoparticles were microscopically identified by field emission transmission electron microscopy (FE-TEM) using a multifunctional 200 kV-operated JEM-2100F (JEOL, Akishima, Tokyo, Japan) and scanning electron microscope (SEM) using Leo Supra 55, Genesis 2000 (Carl Zeiss, Oberkochen, Germany). The particle image was observed on a copper grid by putting a drop of synthesized nanoparticles. To determine the quality and distribution of gold nanoparticles, energy dispersive X-ray spectroscopy (EDX; Bruker, Ewing, NJ, USA) and elemental mapping analysis was applied. Thermo-gravimetric analysis (TGA) was performed using a Baxit thermogravimetric analyzer (Shanghai, China) operated at temperatures ranging 0–600 °C to determine the polymer content on the surface of the CurtoCK-AuNPs. X-ray diffraction analysis (XRD) using a D8 Advance (Bruker, Karlsruhe, Germany) under the condition of 40 kV and 40 mA, and Cu-Kα radiation ($\lambda = 1.54$ Å) in 2θ range of 20 to 80 was applied to confirm the information of the nanoparticles' crystalline structure, phase nature, lattice characteristics, and crystalline grain size. The Scherrer equation to compute the average crystal diameter of gold nanoparticles was calculated as follow equation: $D = k\,\lambda/\beta\,\cos\theta$, where D highlights crystalline size of the particles; k is the Scherrer constant, equal to the shape factor 0.9; the wavelength of light diffraction is λ (where $\lambda = 1.54$ Å); β is the full-width at half-maximum (FWHM); and θ is the Bragg angle of refraction. Dynamic light scattering (DLS) was performed to investigate the volume and intensity of nanoparticles using the ELSZ-2000 series (Otsuka Electronics Co., Osaka, Japan).

Evaluation of in vitro cell cytotoxicity of nanoparticles

Murine macrophages (RAW264.7), human stomach adenocarcinoma (AGS), and human keratinocytes (HaCaT) were obtained from Korean Cell Line Bank (KCLB, Seoul, Korea). AGS cells were cultured in RPMI medium, whereas RAW264.7 and HaCaT cells were cultured in DMEM. Both media contained 10% FBS and 1% PS, and all cells were incubated at 37 °C in a humidified incubator (Shenzhen, Guangdong, China) under 95% air/5% CO_2 conditions. To identify the cytotoxic effect of nanoparticles, each cell line

was plated at a density of 1×10^4 cells/well in a 96-well plate (SPL Life Science, Pocheon, Republic of Korea). The cells were washed twice with PBS after 24 h of incubation, and serum-free media containing various concentrations of the samples was added to the cells. Cell viability was evaluated using a commercial MTT solution after a further 24 h incubation. The optical density was measured at 570 nm using a SpectraMax® ABS plus machine (San Jose, CA, USA). Each sample's cell viability was evaluated as a percentage of control cells treated just only medium. For the colony formation analysis, AGS cells (1×10^4 cells/well) were seeded into 6-well plates and stabilized for 24 h. The medium was replaced with fresh serum-free media containing various concentrations of the sample after washing twice with PBS. Following incubation for 3 days, the cells were washed twice with PBS, and well-grown colonies were stained with 0.1% crystal violet solution. After washing with PBS in triplicate, photographs of the cells were captured by inverted light microscopy (Leica DMi8, Wetzlar, Germany), and the number of colonies was counted.

Live and dead cell staining with Hoechst and PI dye

AGS cells (1×10^6 cells/well) were seeded into 6-well plates and incubated for 24 h, containing different concentrations of the sample. Following incubation for an additional 24 h, the cells were washed twice with PBS and stained with Hoechst 33258 (10 μg/mL) and PI (5 μg/mL) solutions, respectively, at room temperature for 30 min. The live and dead cells were visually identified using a Leica DMLB fluorescence microscope (Leica, Wetzlar, Germany).

Mitochondrial staining with MitoTracker fluorescent dye

For mitochondrial staining, MitoTracker™ Green FM (Cell Signaling Technology, Danvers, MA, USA) was utilized. AGS cells (1×10^6 cells) were grown on 22-mm^2 coverslips in 6-well plates and incubated overnight for stabilization. After washing twice with PBS, various concentrations of the sample were treated. After incubation for 24 h, the cells were washed twice with PBS and stained with 1 mL of prewarmed medium containing 50 nM MitoTracker™ Green solution for 30 min. A Leica DM IRM inverted modulation contrast microscope (Leica Microsystems, Bustleton Pike Feasterville, PA, USA) was used to visually identify the stained cells.

Quantitative real-time PCR analysis

The AGS cells treated with the samples were harvested using a Tris reagent (Meridian Bioscience, Cincinnati, OH, USA) and a HelixCriptTM Easy cDNA Synthesis Kit was used to make cDNA from whole RNA (Nanohelix, Daejeon, Republic of Korea). Quantitative real-time PCR (qRT-PCR) was performed using a RealHelix™ Premier qPCR Kit (Nanohelix, Daejeon, Republic of Korea) on a PCR Rotor-Gene Q (Qiagen, Hilden, Germany). All samples were tested in triplicate using β-actin as a standard. All the primers were designed from Macrogen (Seoul, Republic of Korea), and Additional file 1: Table S1 lists the gene-specific primers utilized in this study.

Western blotting analysis

Total proteins of the AGS cells treated with the samples were extracted using RIPA lysis buffer (Abcam, Cambridge, UK). Protein content was quantified and standardized using a Bio-Rad protein assay kit (Bio-Rad Laboratories Inc., Hercules, CA, USA). Total protein was separated by 10% sodium dodecyl sulfate-polyacrylamide gel electrophoresis (SDS-PAGE), and the separated proteins were transferred onto a polyvinylidene fluoride (PVDF) membrane (EMD Millipore, Billerica, MA, USA). Then membrane was blocked for 1 h with Tris-buffered saline (pH 7.0) containing 5% skim milk, then washed three times with PBS containing 0.1 percent Tween 20-contained PBS (PBST). Then primary antibodies were incubated overnight at 4 °C followed by secondary antibodies for 2 h at room temperature. After washing the membrane with PBST several times, the ECL substrate solution was treated and protein bands were visualized using an ATTO LuminiGraph III lite chemiluminescence gel imaging system (Atto, Tokyo, Japan). Each band size and sensitivity were quantified using the Image J program (National Institute of Health, Bethesda, MD, USA), and results were calculated as relative expression against the band of β-actin used as a housekeeping protein.

Statistical analysis

Results were presented as the mean ± standard deviation (SD) of three independent experiments triplicate. Statistical analyses were performed by Student's *t*-test using PASW Statistics 18 (IBM Co., Armonk, NY, USA). A significant difference was considered at a p-value threshold of < 0.05 between two groups.

Results

Biosynthesis and physiochemical characterization of CurtoCK-AuNPs

In the present study, to investigate the anti-GC activity of CK-gold nanoparticles, we used *C. proimmune* K3 strain that was isolated from fermented ginseng beverage and was reported in our previous study (Dhandapani et al. 2021). Compound K is known to have low water solubility, but is highly dissolved in DMSO up to a concentration of 100 mg/mL (approximately 1.6 mM). Because we used compound K at concentrations below 0.3 mM in this study, it was obviously dissolved in DMSO. Gold nanoparticles (CurtoCK-AuNPs) of CK were successfully synthesized via the biotransformation of *C. proimmune* K3 and gold salts. We obtained CurtoCK-AuNPs with high dispersibility and stability without any precipitated materials, after mixing compound K with *Curtobacterium* suspension and gold salt, as shown in the photos of Fig. 1. The optimal conditions for the synthesis of CurtoCK-AuNPs were monitored with respect to incubation time, concentration of CK and $HAuCl_4$, and reaction pH. By visually observing the color change to purple and measuring absorbance, the synthesis method was optimized. As shown in Fig. 1, optimal conditions for successful CurtoCK-AuNPs synthesis were as follows: 0.25 mM CK, 2 mM gold salts, 1×10^3 CFU/mL *C. proimmune* K3, pH 6.0, and for 2 days incubation. UV–Vis spectroscopy to observe the maximal absorption of CurtoCK-AuNPs determined that the λ_{max} value was at 545 nm.

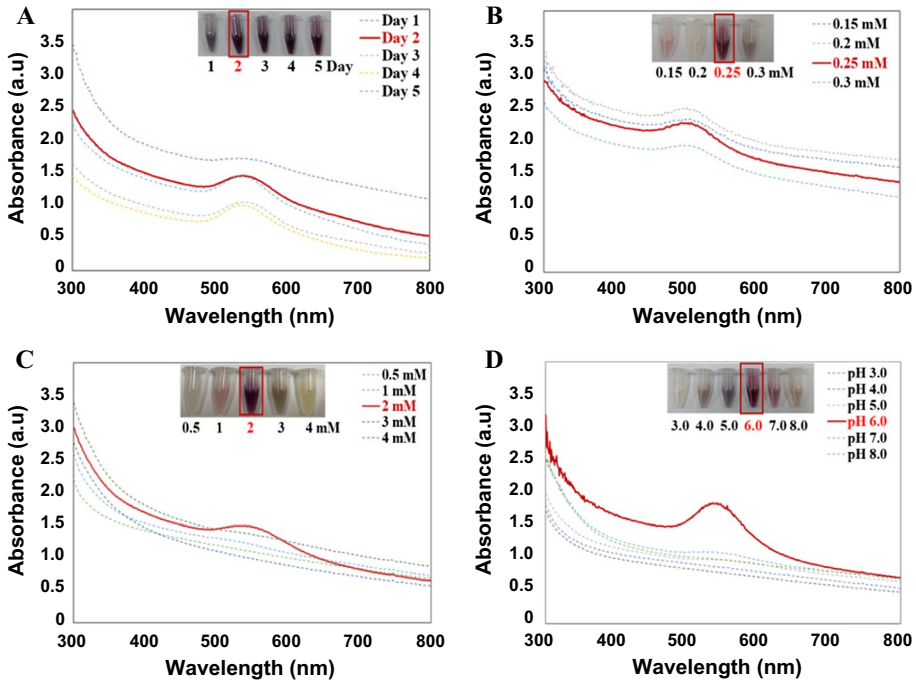

Fig. 1 Scanning of UV–Vis spectra to establish the optimal conditions for biosynthesis of CurtoCK-AuNPs, depending on **A** reaction times; **B** concentrations of compound K; **C** concentrations of gold salts; and **D** ranges of reaction pH. The optimized method was established by visually observing change of color from yellow to deep purple and measuring absorbance at 300–800 nm. The red solid lines in each spectrum were decided as the optimal condition for each parameter, based on the maximal absorption at the λ_{max} (545 nm)

Physicochemical characterization of CurtoCK-AuNPs

The morphological and physicochemical characteristics of CurtoCK-AuNPs were identified by FE-TEM analysis. The synthesized CurtoCK-AuNPs displayed mainly spherical-shaped AuNPs around 200 nm in size (Fig. 2A). Elemental mapping analysis showed a wide distribution of metallic gold, presenting as red dots in the synthesized CurtoCK-AuNPs (Fig. 2B). Figure 2C shows that the SAED spectrum recorded from the spherical-shaped single crystals could be accurately indexed based on the structure of CurtoCK-AuNPs. The EDX spectrum showed that CurtoCK-AuNPs had strong and abundant signals, especially at 1.9 and 2.1 keV, which correspond to the metallic crystallites in typical gold nanoparticles (Fig. 2D). Meanwhile, the highest optical absorption peaks were observed at 8.0 keV, which typically corresponded to copper atoms, induced by the copper grid used for TEM analysis (Shah et al. 2015). In contrast, Fig. 2E displays representative SEM image of CurtoCK-AuNPs prepared by carbon coating on thin film copper grids. The SEM image showed compact spherical morphologies with the size of 80–100 nm. The particles adhered to each other and formed large agglomerations, suggesting that CurtoCK-AuNPs have surface with high energy.

The results indicated that CurtoCK-AuNPs possess different shapes (spherical, elongated, and rod) with an average size of approximately 80–87 nm. XRD analysis was used to determine the crystallographic structure of the CurtoCK-AuNPs (Fig. 3A). Four major peaks at 2θ angles of 111, 200, 220, and 311 were observed, which corresponded to the face-centered cubic crystal structure of gold lattice planes of Bragg's reflection.

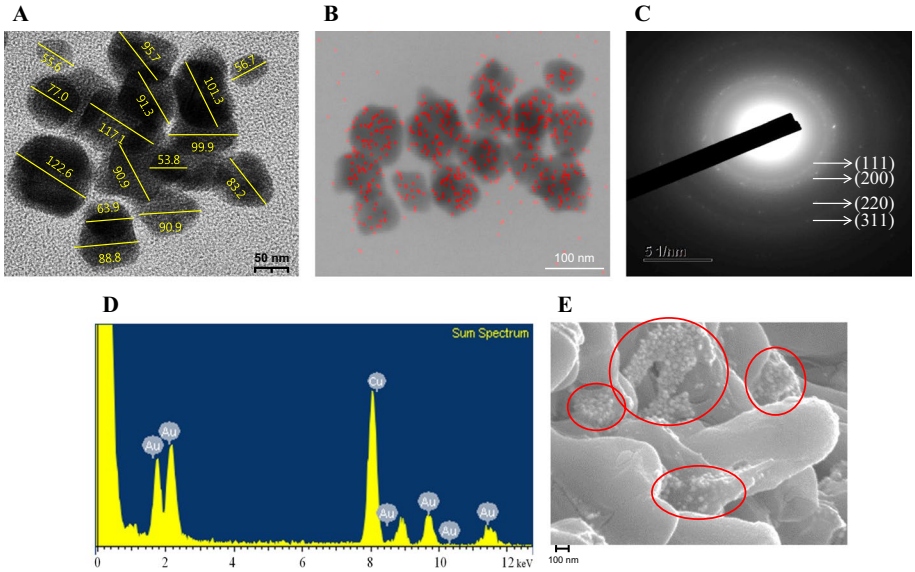

Fig. 2 Physicochemical characterization of CurtoCK-AuNPs. **A** Transmission electron microscopy (TEM) image for determination of morphological characteristics. **B** Electron mapping of CurtoCK-AuNPs. **C** Selected area electron diffraction (SAED) image obtained by TEM analysis for determination of crystalline structure. **D** Energy-dispersive X-ray (EDX) spectrum for determining elemental distribution. **E** Scanning electron microscopy (SEM) image for determination of morphological characteristics of crystalline structure

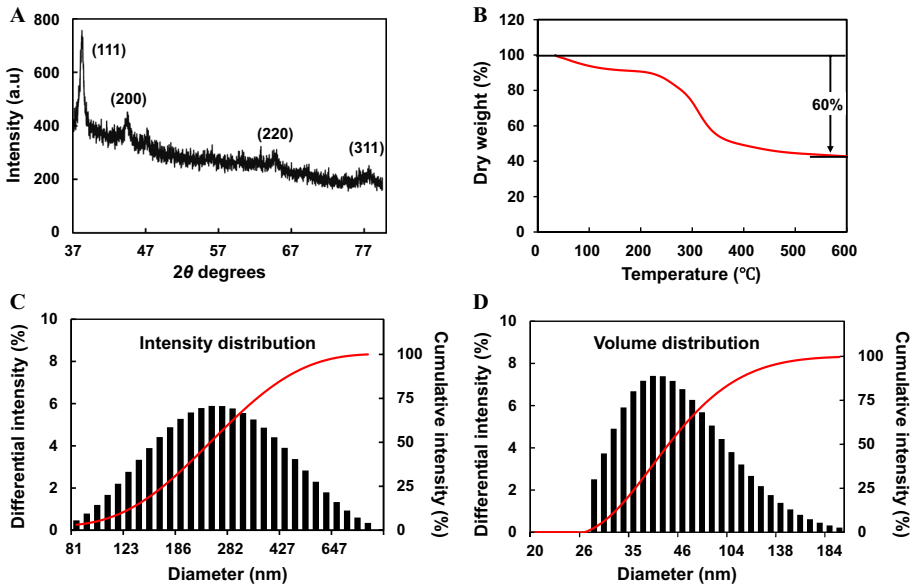

Fig. 3 Physicochemical characterization of CurtoCK-AuNPs. **A** X-ray diffraction (XRD) spectrum for identification of crystalline structure. **B** Thermo-gravimetric analysis (TGA) for determination of thermal stability. **C**, **D** Dynamic light scattering (DLS) spectrum for determination of intensity and volume distributions of CurtoCK-AuNPs

To estimate the thermal stability of the CurtoCK-AuNPs, TGA was performed at temperatures ranging from 0 to 600 °C. As shown in Fig. 3B, the result indicated that weight loss of CurtoCK-AuNPs decreased slightly at temperatures between 50 and 200 °C, but

dramatically decreased at temperatures ranges above 200 °C to 400 °C. At a temperature of 600 °C, weight loss of CurtoCK reached approximately 60%. To estimate the size distribution profiles of CurtoCK-AuNPs, DLS spectroscopy was applied. The size distribution of CurtoCK-AuNPs was observed to be approximately 85–800 (average 240 nm) nm for intensity distribution (Fig. 3C) and 30–190 nm (maximum 40 nm) for volume distribution (Fig. 3D), respectively. DLS spectroscopy also indicated that the polydispersity index and zeta potential value of CurtoCK-AuNPs were 0.29 and − 22.5 mV, respectively. The results suggest that CurtoCK-AuNPs had a moderate polydispersive and relatively stable characteristics.

Cytotoxic effect of CurtoCK-AuNPs

First, we measured the cytotoxic effect of CurtoCK-AuNPs on two types of normal cells, including HaCaT human keratinocytes and RAW 264.7 murine macrophages.

Figure 4A, B shows that, neither CurtoCK-AuNPs nor *C. proimmune* K3 showed significant toxic effects (above 80% viability) on HaCaT and RAW 264.7 cells at concentrations ranging from 100 to 400 µg/mL. Next, their cytotoxic effects on AGS human gastric carcinoma cells were estimated (Fig. 4C). Although *C. proimmune* K3 did not show a significant toxic effect against AGS cells, CurtoCK-AuNPs exerted dose-dependent cytotoxic effects against AGS cells. In particular, significant toxic effects were observed in the cells treated with CurtoCK-AuNPs at doses from 200 to 400 µg/mL (approximately 50% to 70% cytotoxicity). In addition, the colonies of AGS cells treated with CurtoCK-AuNPs were stained with crystal violet dye, and the results were presented as morphological images and their quantification (Fig. 4D). Compared with untreated control cells,

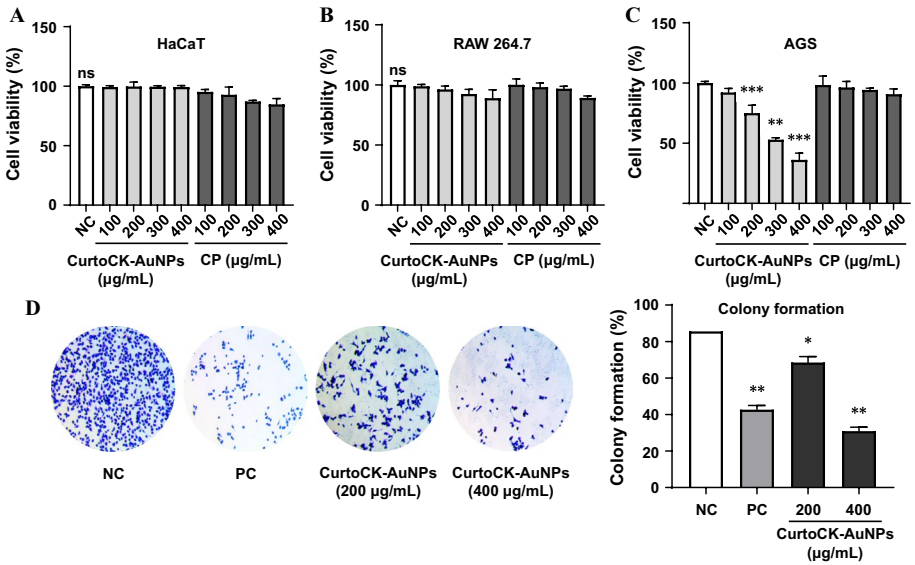

Fig. 4 Cytotoxic effect of nanoparticles (CurtoCK-AuNPs) and *C. proimmune* K3 (CP) on normal and cancer cells. **A** HaCaT human keratinocytes. **B** RAW264.7 murine macrophage. **C** AGS human gastric cancer cells. The cell viability was evaluated using MTT assay. **D** The microscopic images (magnification ×100) of stained AGS cells treated with CurtoCK-AuNPs for determination of colony formation. Medium alone and cisplatin (50 µM) were used as negative (NC) and positive (PC) controls, respectively. The colony formation was evaluated using crystal violet staining and their quantified results. The asterisks on each column indicate significant difference between NC and each sample. *$p < 0.05$; **$p < 0.01$, ***$p < 0.001$. ns, not significant

the CurtoCK-AuNPs-treated AGS cells induced a significantly toxic effect that was comparable to those observed in 50 μM cisplatin-treated cells, which were used as a positive control (PC).

Mitochondrial damage-induced apoptosis by CurtoCK-AuNPs treatment

The apoptotic cells induced by treatment with CurtoCK-AuNPs was evaluated by fluorescence staining with Hoechst 33258 and PI dyes (Fig. 5A). Compared with untreated control cells that produced few azure-blue colors in response to the staining, both cisplatin (PC) and CurtoCK-AuNPs treatments induced significant production of the azure-blue and red colors during the Hoechst 33258 and PI stainings, respectively, indicating a significant increase in apoptotic cells. In addition, mitochondrial alteration in AGS cells induced by CurtoCK-AuNPs treatment was investigated using MitoTracker staining, a mitochondria-specific fluorescent dye. As illustrated in Fig. 5B, the number of stained mitochondria was dramatically decreased in cisplatin (PC) or CurtoCK-AuNP-treated AGS cells compared with those in control cells. Nuclei were stained blue, whereas green mitochondria were a response to MitoTracker dye. Morphological changes in mitochondria were noticed between control and CurtoCK-AuNP-treated cells, suggesting a mitochondrial alteration.

CurtoCK-AuNPs-induced apoptotic signaling pathway

Based on the above findings, we investigated the expression of genes and proteins related to apoptosis signaling using qRT-PCR and western blotting, respectively.

As shown in Fig. 6, qRT-PCR results showed that dose-dependent alterations in apoptosis-associated genes were observed in AGS cells treated with CurtoCK-AuNPs. CurtoCK-AuNPs treatment significantly upregulated the expression of

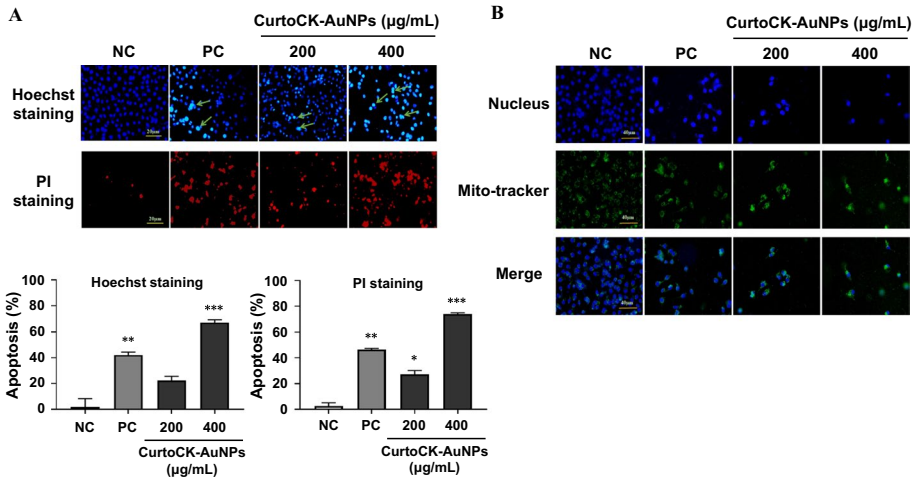

Fig. 5 Fluorescence microscopy images of CurtoCK-AuNP-treated AGS cells stained with **A** Hoechst and propidium iodide dyes. The green arrows in the pictures indicate fragmented nuclei with condensed chromatin, meaning a damaged nucleus. The staining results of were quantified using Image J software. **B** Fluorescence microscopy images of mitochondrial morphology of CurtoCK-AuNP-treated AGS cells stained with MitoTracker dye. Medium alone and cisplatin (50 μM) were used as negative (NC) and positive (PC) controls, respectively. The asterisks on each column indicate significant difference between NC and each sample. *$p < 0.05$, **$p < 0.01$, ***$p < 0.001$

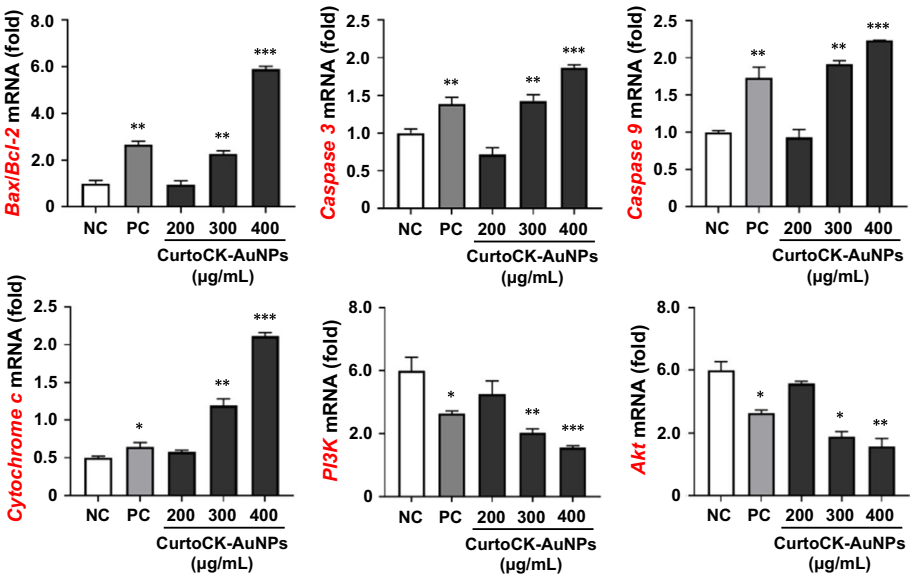

Fig. 6 Effects of CurtoCK-AuNPs on the expression of apoptosis-related genes, including Bax, Bcl-2, cytochrome c, caspase 9, caspase 3, PI3K, and Akt in AGS cells. The expression level of each gene was determined using qRT-PCR. Medium alone and cisplatin (50 μM) were used as negative (NC) and positive (PC) controls, respectively. The asterisks on each column indicate significant difference between NC and each sample. *$p < 0.05$, **$p < 0.01$, ***$p < 0.001$. Bax, Bcl-2-associated X protein; Bcl-2, B cell lymphoma-2; PI3K, phosphoinositide 3-kinase

mRNA, including *Bax*/*Bcl-2*, *caspase 3*, *caspase 9*, and *cytochrome c*, and significantly downregulated the expression of *PI3K* and *Akt*, thereby indicating the induction of apoptosis. Interestingly, no significant difference was observed in any genes when AGS cells were treated with CurtoCK-AuNPs at a low dose of 200 μg/mL, but the gene expression was significantly and dose-dependently upregulated and downregulated at doses above 300 μg/mL. The expression of these genes was verified by evaluating the expression of intracellular proteins using western blot analysis. Representative band images obtained by western blotting are displayed in Fig. 7A, and their quantified results based on band images are provided in Fig. 7B. Consequently, these results of gene expression mirror the tendencies shown in Fig. 6, supporting the assertion that intracellular proteins were significantly regulated by CurtoCK-AuNPs treatment in AGS cells. In other words, significant upregulations of Bax/Bcl-2, cytochrome c, cleaved caspase 3/caspase 3, and cleaved caspase 9/cleaved caspase 9 were observed in a dose-dependent manner, whereas phosphorylation of PI3K and Akt was significantly downregulated in AGS cells treated with CurtoCK-AuNPs, suggesting the induction of apoptosis in the cells. Nevertheless, inconsistency was observed between genes and proteins expressions in apoptosis-related biomarkers of the cells treated with CurtoCK-AuNPs at a concentration of 200 μg/mL (Figs. 6, 7). These phenomena occur possibly because apoptosis-related gene expressions were already downregulated to steady-state levels after activation by treating CurtoCK-AuNPs at a 200 μg/mL concentration.

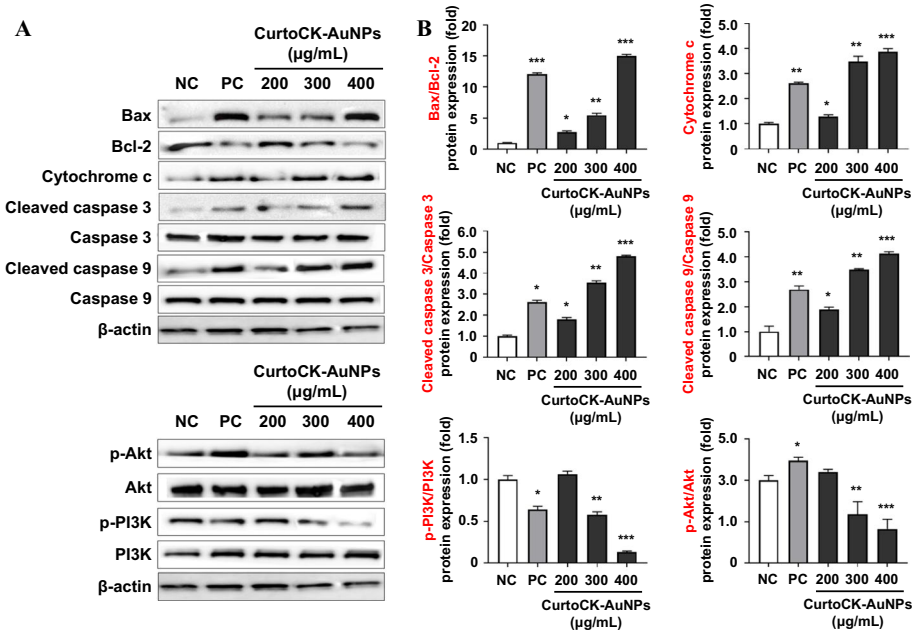

Fig. 7 Effect of CurtoCK-AuNPs on the expression of apoptosis-related proteins, including Bax, Bcl-2, cytochrome c, caspase 9, caspase 3, PI3K, and Akt in AGS cells. **A** The expression level of each gene was determined by western blotting, and **B** their blotting images were quantified using Image J software. Medium alone and cisplatin (50 μM) were used as negative (NC) and positive (PC) controls, respectively. The asterisks on each column indicate significant difference between NC and each sample. *$p < 0.05$, **$p < 0.01$, ***$p < 0.001$. *Bax* Bcl-2-associated X protein, *Bcl-2* B cell lymphoma-2, *PI3K* phosphoinositide 3-kinase

Discussion

By examining various synthesis conditions, the optimal condition for the biosynthesis of CurtoCK-AuNPs was established when 0.25 mM CK and 2 mM $HAuCl_4$ were added to the suspension of *C. proimmune* K3 (1×10^3) cells, followed by incubation for 2 days at pH 6.0 and 37 ℃ (Fig. 1). CK and microorganisms can be used to synthesize AuNPs, which can be easily visualized changing of color from yellow to deep purple (Shakeel et al. 2016). Recently, Kim et al. (2019) demonstrated a gold nanoparticle, named DCY51T-AuCKNps, prepared by one-pot biosynthesis using *Lactobacillus kimchicus* DCY51T and CK, but to the best of our knowledge, this study is the first to study biosynthesized AuNPs using *Curtobacterium proimmune* K3 and ginsenoside CK (Kim et al. 2019). The synthesized CurtoCK-AuNPs were characterized, using various microscopic and spectrometric analyses, including FE-TEM, SAED, EDX, SEM, DLS and XRD, and found gold nanoparticles having a characteristic spherical shape and an average size of around 200 nm (Figs. 2, 3). In particular, TEM analysis displayed the surface morphology of nanoparticles and clusters of nanoparticles with strong binding forces, whereas SEM analysis showed that nanoparticles mainly bound to the bacterial surface. Given the synthesis mechanism of gold nanoparticles, some hypotheses have been proposed regarding the mechanism of biosynthesis of AuNPs, but the precise mechanisms are still unclear (Hulkoti and Taranath 2014). In the XRD analysis, the highest planes of 111, 200, 220, and 311 suggested that the synthesized CurtoCK-AuNPs were formulated mainly of crystalline gold particles (Abbai et al. 2016; Patra and Baek 2015). TGA analysis demonstrates that CurtoCK-AuNPs had higher thermal stability at temperatures below 250 °C.

In addition, our study aimed to establish the anticancer potential of CurtoCK-AuNPs and its underlying mechanism in AGS cells. Interestingly, CurtoCK-AuNPs did not show any cytotoxicity against normal cells (HaCaT, and RAW264.7) at the concentrations tested, but it resulted in a significant toxic effect on AGS cells, demonstrating that CurtoCK-AuNPs exhibited selective cytotoxicity in cancer cells without affecting normal cells (Fig. 4). Moreover, the result that only *C. proimmune* K3 did not exert cytotoxic effect on the cells, indicating that anticancer activity can be generated via biological synthesis of *C. proimmune* K3 into gold nanoparticles.

Hoechst and PI staining, which can be utilized to easily observe apoptotic cell morphologies, showed that CurtoCK-AuNPs induced significant apoptosis in AGS cells in a dose-dependent manner (Fig. 5A). Further, MitoTracker staining result suggested that the CurtoCK-AuNP-induced apoptosis might happened due to induction of mitochondrial disruption in AGS cells (Fig. 5B). Of the two major apoptotic pathways, the intrinsic (mitochondrial) pathway caused by mitochondrial alterations involves conserved signaling proteins, including Bax, Bcl-2, cytochrome c, and the caspase family (Leibowitz and Yu 2010; Nandhini et al. 2020). Briefly, from several exogenous and endogenous stimuli, the intrinsic apoptosis pathway facilitates the regulation of mitochondrial membrane-bound proteins including Bcl-2 (anti-apoptotic) and Bax (pro-apoptotic). These results in the depletion of mitochondrial outer membrane potential followed by secretion of cytochrome c, which recruits and activates pro-caspase 9, which, in turn, activates the caspase cascade, resulting in cell apoptosis (Loreto et al. 2014). To investigate the intrinsic pathway of apoptosis, gene and protein expression of Bax, Bcl-2, cytochrome c, caspase 9, and caspase 3 were evaluated in AGS cells treated with CurtoCK-AuNPs (Figs. 6, 7). The results showed that CurtoCK-AuNPs treatment significantly upregulated pro-apoptotic genes expression, including Bax, cytochrome c, caspase 9, and caspase 3, but significantly downregulated the anti-apoptotic Bcl-2 gene, demonstrating apoptosis-induced cytotoxicity against AGS cells. A similar investigation was reported by Yun et al. (2020), who demonstrated the influence of gold nanoparticles (VN-AuNPs) prepared from *Vitex negundo* in their pro-apoptotic effect against AGS cells (Yun et al. 2020). Additionally, we further investigated whether CurtoCK-AuNPs can affect PI3K/Akt signaling in AGS cells, a key regulator of survival/proliferation or apoptosis of cancer (Martini et al. 2014). As the inhibition of apoptosis needs survival of cells that is accompanied by inhibiting pro-apoptotic mediator's expression as well as promoting the expression of anti-apoptotic mediators PI3K/Akt signaling that play a crucial role in suppressing intrinsic apoptosis (Senthilkumar and Kim 2013; Wang and Youle 2009), and its activation has been reported in 30–60% of all tumors, including GC (Markman et al. 2010). Our results demonstrated that CurtoCK-AuNPs significantly downregulated PI3K and Akt expression of mRNA in AGS cells in a dose-dependent manner, suggesting that CurtoCK-AuNPs induced apoptotic cell cytotoxicity in AGS cells through the suppression of PI3K/Akt signaling pathway. Furthermore, similar trends were observed with respect to the protein levels; CurtoCK-AuNPs treatment significantly upregulated pro-apoptotic proteins expression, including Bax, cytochrome c, cleaved caspase 9/caspase 9, and cleaved caspase 3/caspase 3, in a dose-dependent manner. These proteins significantly downregulated the expression of anti-apoptotic proteins,

including p-PI3K, p-Akt, and Bcl-2. Above all, our results showed that CurtoCK-AuNPs can exert anticancer activity against GC by upregulating apoptotic signaling and suppressing the PI3K/Akt signaling pathway.

Conclusion

CurtoCK-AuNPs were prepared with ginsenoside CK and $HAuCl_4.3H_2O$ via microbial biosynthesis using a novel bacterial strain, *Curtobacterium proimmune* K3. The optimized synthesis conditions were determined, and the physiochemical characteristics of CurtoCK-AuNPs were identified using various analytical methods, such as UV–Vis spectrometry, FE-TEM, EDX, elemental mapping, XRD, SAED, and DLS spectroscopy. CurtoCK-AuNPs exerted significant cytotoxic effects on AGS cells without toxic effects on normal cells, suggesting that CurtoCK-AuNPs may be safely used as a target for anticancer treatment. CurtoCK-AuNPs exhibited anticancer effects via the underlying pathway of intrinsic apoptosis, being associated with activation of Bax/Bcl-2, cytochrome c, caspase 9, and caspase 3, as well as suppressing PI3K–Akt signaling. To the best of our knowledge, the present study is the first to demonstrate that CurtoCK-AuNPs may serve as a therapeutic agent for GC treatment. Furthermore, our study generated preliminary data for developing innovative anticancer candidates and understanding their mechanisms, thereby providing a good fundamental idea for the development of alternative medications based on using gold nanoparticle of ginseng-derived CK.

Supplementary Information

The online version contains supplementary material available at https://doi.org/10.1186/s12645-022-00133-y.

Additional file 1: Table S1. Primer sequences used in this study.

Acknowledgements
Not applicable.

Author contributions
AMP prepared nanoparticle sample. AMP and RW cultured and maintained the animal cells and evaluated anticancer activity of the sample. AMP, XX and HK did analytical methods for characterization of the sample. AMP, XX and HK analyzed and validated the raw data and prepared the figures. AMP and HK wrote the original draft of manuscript, and HK and YJK reviewed and revised the manuscript. YJK supervised overall process of the experiment. All authors read and approved the final manuscript.

Funding
This work was supported by a grant from the Basic Science Research Program through the National Research Foundation of Korea funded by the Ministry of Education (2019R1A2C1010428) and also supported by KDBIO Corp.

Availability of data and materials
Not applicable.

Declarations

Ethics approval and consent to participate
Not applicable.

Consent for publication
Not applicable.

Competing interests
The authors declare that they have no competing interests.

Received: 23 May 2022 Accepted: 26 August 2022
Published online: 13 September 2022

References

Abbai R, Mathiyalagan R, Markus J, Kim YJ, Wang C, Singh P, Ahn S, Farh Mel A, Yang DC (2016) Green synthesis of multifunctional silver and gold nanoparticles from the oriental herbal adaptogen: Siberian ginseng. Int J Nanomed 11:3131–3143. https://doi.org/10.2147/ijn.S108549

Akao T, Kida H, Kanaoka M, Hattori M, Kobashi K (1998) Intestinal bacterial hydrolysis is required for the appearance of compound K in rat plasma after oral administration of ginsenoside Rb1 from *Panax ginseng*. J Pharm Pharmacol 50:1155–1160. https://doi.org/10.1111/j.2042-7158.1998.tb03327.x

Bhattacharya R, Mukherjee P (2008) Biological properties of "naked" metal nanoparticles. Adv Drug Deliv Rev 60:1289–1306. https://doi.org/10.1016/j.addr.2008.03.013

Bray F, Ferlay J, Soerjomataram I, Siegel RL, Torre LA, Jemal A (2018) Global cancer statistics 2018: GLOBOCAN estimates of incidence and mortality worldwide for 36 cancers in 185 countries. CA Cancer J Clin 68:394–424. https://doi.org/10.3322/caac.21492

Cai W, Gao T, Hong H, Sun J (2008) Applications of gold nanoparticles in cancer nanotechnology. Nanotechnol Sci Appl 1:17–32. https://doi.org/10.2147/nsa.s3788

Cao Z, Liu J (2020) Bacteria and bacterial derivatives as drug carriers for cancer therapy. J Control Release 326:396–407. https://doi.org/10.1016/j.jconrel.2020.07.009

Cao Z, Cheng S, Wang X, Pang Y, Liu J (2019) Camouflaging bacteria by wrapping with cell membranes. Nat Commun 10:3452. https://doi.org/10.1038/s41467-019-11390-8

Chase AB, Arevalo P, Polz MF, Berlemont R, Martiny JBH (2016) Evidence for ecological flexibility in the cosmopolitan genus *Curtobacterium*. Front Microbiol 7:1874. https://doi.org/10.3389/fmicb.2016.01874

Dang Y, Liu T, Yan J, Reinhardt JD, Yin C, Ye F, Zhang G (2020) Gastric cancer proliferation and invasion is reduced by macrocalyxin C via activation of the miR-212-3p/Sox6 pathway. Cell Signal 66:109430. https://doi.org/10.1016/j.cellsig.2019.109430

Davis ME, Chen Z, Shin DM (2008) Nanoparticle therapeutics: an emerging treatment modality for cancer. Nat Rev Drug Discov 7:771–782. https://doi.org/10.1038/nrd2614

Dhandapani S, Xu X, Wang R, Puja AM, Kim H, Perumalsamy H, Balusamy SR, Kim Y-J (2021) Biosynthesis of gold nanoparticles using *Nigella sativa* and *Curtobacterium proimmune* K3 and evaluation of their anticancer activity. Mater Sci Eng C 127:112214. https://doi.org/10.1016/j.msec.2021.112214

Funke G, Aravena-Roman M, Frodl R (2005) First description of *Curtobacterium* spp. isolated from human clinical specimens. J Clin Microbiol 43:1032–1036. https://doi.org/10.1128/JCM.43.3.1032-1036.2005

Gowramma B, Keerthi U, Rafi M, Muralidhara Rao D (2015) Biogenic silver nanoparticles production and characterization from native stain of *Corynebacterium* species and its antimicrobial activity. 3 Biotech 5:195–201. https://doi.org/10.1007/s13205-014-0210-4

Grasso G, Zane D, Dragone R (2019) Microbial nanotechnology: challenges and prospects for green biocatalytic synthesis of nanoscale materials for sensoristic and biomedical applications. Nanomaterials 10:11. https://doi.org/10.3390/nano10010011

Heiligtag FJ, Niederberger M (2013) The fascinating world of nanoparticle research. Mater Today 16:262–271. https://doi.org/10.1016/j.mattod.2013.07.004

Herizchi R, Abbasi E, Milani M, Akbarzadeh A (2016) Current methods for synthesis of gold nanoparticles. Artif Cells Nanomed Biotechnol 44:596–602. https://doi.org/10.3109/21691401.2014.971807

Hulkoti NI, Taranath TC (2014) Biosynthesis of nanoparticles using microbes—a review. Colloids Surf B 121:474–483. https://doi.org/10.1016/j.colsurfb.2014.05.027

Kim YJ, Perumalsamy H, Markus J, Balusamy SR, Wang C, Ho Kang S, Lee S, Park SY, Kim S, Castro-Aceituno V, Kim SH, Yang DC (2019) Development of *Lactobacillus kimchicus* DCY51(T)-mediated gold nanoparticles for delivery of ginsenoside compound K: in vitro photothermal effects and apoptosis detection in cancer cells. Artif Cells Nanomed Biotechnol 47:30–44. https://doi.org/10.1080/21691401.2018.1541900

Lamprecht A, Ubrich N, Yamamoto H, Schäfer U, Takeuchi H, Maincent P, Kawashima Y, Lehr C-M (2001) Biodegradable nanoparticles for targeted drug delivery in treatment of inflammatory bowel disease. J Pharmacol Exp Ther 299:775–781

Leibowitz B, Yu J (2010) Mitochondrial signaling in cell death via the Bcl-2 family. Cancer Biol Ther 9:417–422. https://doi.org/10.4161/cbt.9.6.11392

Liu R, Cao Z, Wang L, Wang X, Lin S, Wu F, Pang Y, Liu J (2022) Multimodal oncolytic bacteria by coating with tumor cell derived nanoshells. Nano Today 45:101537. https://doi.org/10.1016/j.nantod.2022.101537

Loreto C, La Rocca G, Anzalone R, Caltabiano R, Vespasiani G, Castorina S, Ralph DJ, Cellek S, Musumeci G, Giunta S, Djinovic R, Basic D, Sansalone S (2014) The role of intrinsic pathway in apoptosis activation and progression in Peyronie's disease. Biomed Res Int 2014:616149. https://doi.org/10.1155/2014/616149

Markman B, Atzori F, Pérez-García J, Tabernero J, Baselga J (2010) Status of PI3K inhibition and biomarker development in cancer therapeutics. Ann Oncol 21:683–691. https://doi.org/10.1093/annonc/mdp347

Martini M, De Santis MC, Braccini L, Gulluni F, Hirsch E (2014) PI3K/AKT signaling pathway and cancer: an updated review. Ann Med 46:372–383. https://doi.org/10.3109/07853890.2014.912836

Nandhini JT, Ezhilarasan D, Rajeshkumar S (2020) An ecofriendly synthesized gold nanoparticles induces cytotoxicity via apoptosis in HepG2 cells. Environ Toxicol 36:24–32. https://doi.org/10.1002/tox.23007

Patra JK, Baek K-H (2015) Novel green synthesis of gold nanoparticles using *Citrullus lanatus* rind and investigation of proteasome inhibitory activity, antibacterial, and antioxidant potential. Int J Nanomed 10:7253–7264. https://doi.org/10.2147/IJN.S95483

Puvanakrishnan P, Park J, Chatterjee D, Krishnan S, Tunnell JW (2012) *In vivo* tumor targeting of gold nanoparticles: effect of particle type and dosing strategy. Int J Nanomed 7:1251–1258. https://doi.org/10.2147/ijn.S29147
Rónavári A, Igaz N, Adamecz DI, Szerencsés B, Molnar C, Kónya Z, Pfeiffer I, Kiricsi M (2021) Green silver and gold nanoparticles: biological synthesis approaches and potentials for biomedical applications. Molecules 26:844. https://doi.org/10.3390/molecules26040844
Salapa J, Bushman A, Lowe K, Irudayaraj J (2020) Nano drug delivery systems in upper gastrointestinal cancer therapy. Nano Converg 7:38. https://doi.org/10.1186/s40580-020-00247-2
Sekhon BS (2014) Nanotechnology in agri-food production: an overview. Nanotechnol Sci Appl 7:31–53. https://doi.org/10.2147/NSA.S39406
Senthilkumar K, Kim S-K (2013) Cell survival and apoptosis signaling as therapeutic target for cancer: marine bioactive compounds. Int J Mol Sci 14:2334–2354. https://doi.org/10.3390/ijms14022334
Shah M, Fawcett D, Sharma S, Tripathy SK, Poinern GEJ (2015) Green synthesis of metallic nanoparticles via biological entities. Materials 8:7278–7308. https://doi.org/10.3390/ma8115377
Shakeel A, Annu SI, Salprima YS (2016) Biosynthesis of gold nanoparticles: a green approach. J Photochem Photobiol B 161:141–153. https://doi.org/10.1016/j.jphotobiol.2016.04.034
Sharma A, Lee H-J (2020) Ginsenoside compound K: insights into recent studies on pharmacokinetics and health-promoting activities. Biomolecules 10:1028. https://doi.org/10.3390/biom10071028
Shunmugam R, Renukadevi Balusamy S, Kumar V, Menon S, Lakshmi T, Perumalsamy H (2021) Biosynthesis of gold nanoparticles using marine microbe (*Vibrio alginolyticus*) and its anticancer and antioxidant analysis. J King Saud Univ Sci 33:101260. https://doi.org/10.1016/j.jksus.2020.101260
Smalley SR, Benedetti JK, Haller DG, Hundahl SA, Estes NC, Ajani JA, Gunderson LL, Goldman B, Martenson JA, Jessup JM, Stemmermann GN, Blanke CD, Macdonald JS (2012) Updated analysis of SWOG-directed intergroup study 0116: a phase III trial of adjuvant radiochemotherapy versus observation after curative gastric cancer resection. J Clin Oncol 30:2327–2333. https://doi.org/10.1200/JCO.2011.36.7136
Sperling RA, Rivera Gil P, Zhang F, Zanella M, Parak WJ (2008) Biological applications of gold nanoparticles. Chem Soc Rev 37:1896–1908. https://doi.org/10.1039/b712170a
Su H, Wang Y, Gu Y, Bowman L, Zhao J, Ding M (2018) Potential applications and human biosafety of nanomaterials used in nanomedicine. J Appl Toxicol 38:3–24. https://doi.org/10.1002/jat.3476
Sýkora D, Kasicka V, Miksík I, Rezanka P, Záruba K, Matejka P, Král V (2010) Application of gold nanoparticles in separation sciences. J Sep Sci 33:372–387. https://doi.org/10.1002/jssc.200900677
Tiwari PM, Vig K, Dennis VA, Singh SR (2011) Functionalized gold nanoparticles and their biomedical applications. Nanomaterials 1:31–63. https://doi.org/10.3390/nano1010031
Torres-Chavolla E, Ranasinghe RJ, Alocilja EC (2010) Characterization and functionalization of biogenic gold nanoparticles for biosensing enhancement. IEEE Trans Nanotechnol 9:533–538. https://doi.org/10.1109/TNANO.2010.2052926
Wang C, Youle RJ (2009) The role of mitochondria in apoptosis. Annu Rev Genet 43:95–118. https://doi.org/10.1146/annurev-genet-102108-134850
Wang L, Cao Z, Zhang M, Lin S, Liu J (2022) Spatiotemporally controllable distribution of combination therapeutics in solid tumors by dually modified bacteria. Adv Mater 34:e2106669. https://doi.org/10.1002/adma.202106669
Yang Z, Wang JR, Niu T, Gao S, Yin T, You M, Jiang ZH, Hu M (2012) Inhibition of P-glycoprotein leads to improved oral bioavailability of compound K, an anticancer metabolite of red ginseng extract produced by gut microflora. Drug Metab Dispos 40:1538–1544. https://doi.org/10.1124/dmd.111.044008
Yun Z, Chinnathambi A, Alharbi SA, Jin Z (2020) Biosynthesis of gold nanoparticles using *Vitex negundo* and evaluation of pro-apoptotic effect on human gastric cancer cell lines. J Photochem Photobiol B 203:111749. https://doi.org/10.1016/j.jphotobiol.2019.111749
Zhang B, Zhu X-M, Hu J-N, Ye H, Luo T, Liu X-R, Li H-Y, Li W, Zheng Y-N, Deng Z-Y (2012) Absorption mechanism of ginsenoside compound K and its butyl and octyl ester prodrugs in Caco-2 cells. J Agric Food Chem 60:10278–10284. https://doi.org/10.1021/jf303160y
Zhang J, Wang Y, Jiang Y, Liu T, Luo Y, Diao E, Cao Y, Chen L, Zhang L, Gu Q, Zhou J, Sun F, Zheng W, Liu J, Li X, Hu W (2018) Enhanced cytotoxic and apoptotic potential in hepatic carcinoma cells of chitosan nanoparticles loaded with ginsenoside compound K. Carbohydr Polym 198:537–545. https://doi.org/10.1016/j.carbpol.2018.06.121

Publisher's Note